NUMERICAL SIMULATION OF THE TWO-DIMENSIONAL INCOMPRESSIBLE FLOW AROUND AN ELLIPTIC CYLINDER USING THE VORTEX METHOD

Carolina Wigg de Araujo
Promon Engenharia Ltda – Praia do Flamengo 154, 13°andar,Flamengo, Rio de Janeiro, RJ, Brazil, CEP:22207-900
carolina.wigg@promon.com.br

Vanessa G. Guedes
Special Technologies Department, CEPEL – C.P. 68007, Rio de Janeiro, RJ, Brazil, CEP:21944-970
vanessag@cepel.br

Gustavo C. R. Bodstein
Department of Mechanical Engineering, EE/COPPE/UFRJ – C.P. 68503, Rio de Janeiro, RJ, Brazil, CEP:21945-970
gustavo@serv.com.ufrj.br

Abstract. The study of external incompressible flows at high Reynolds numbers around bluff bodies finds extensive applicability to real-life problems, in addition to the scientific interest as a means for testing numerical algorithms. For a wide range of Reynolds numbers such flows are characterized by the formation of a Von Karman-type periodic wake. The occurrence of flow separation makes the prediction of these flows very difficult, and one has to rely on experimental data to calculate the aerodynamic forces on the body. Many attempts to numerically simulate the flow details have been reported in the literature, and a variety of both mesh-based and mesh-free methods have been used. In this paper we use a new mesh-free two-dimensional discrete vortex method to simulate the high Reynolds number flow around an elliptic cylinder. Lamb vortices are generated along the cylinder surface, whose strengths are determined to ensure that the no-slip condition is satisfied and that circulation is conserved. The impermeability condition is imposed through the application of a source panel method, so that mass conservation is explicitly enforced. The dynamics of the body wake is computed using the convection-diffusion splitting algorithm, where the diffusion process is simulated using the random walk method, and the convection process is carried out with a lagrangian first-order time-marching scheme. Results for the time history of the lift and drag coefficients as well as pressure coefficient distribution on the body surface are presented and compared to other results available in the literature.

Keywords: *Aerodynamics, Fluid Mechanics, Bluff Body, Elliptic Cylinder, Vortex Method, Panel Method*

1.Introduction

The study of external incompressible flows at high Reynolds numbers around bluff bodies finds technological applications to real-life engineering problems. For instance, an elliptic cylinder may occur due to a change in the cross section of a circular cylinder due to mechanical deformation or accumulation of material, such as ice. From a scientific point of view, the study of this class of flows is also important for testing numerical algorithms. Flows around bluff bodies are characterized by the occurrence of massive boundary layer separation and the formation of an unsteady, turbulent, periodic wake downstream of the body. These complex phenomena make the numerical prediction of these flows very difficult, and one has to rely on specific experimental data to calculate the aerodynamic forces on the body. Many attempts to numerically simulate most of the flow details have been reported in the literature, and a variety of both mesh-based and mesh-free methods have been used (Chorin, 1973; He and Su, 1998; Leonard, 1980).

The objective of this work is to use the Vortex Method associated with the Panel Method (Pereira, 1999) to simulate the two-dimensional, incompressible, unsteady flow past elliptic cylinders, for four different aspect ratios. The flowfield is calculated as the sum of a uniform flow, a cloud of vortices that model the vorticity in the boundary layer and wake, and a series of piecewise-continuous linear-strength sources distributed on straight panels arranged along the body surface. In our Lagrangian mesh-free vortex method, Lamb vortices are generated along the cylinder surface, whose strengths are determined to ensure that the no-slip condition is satisfied and that circulation is conserved. The impermeability condition is imposed through the application of the source panel method (Anderson, 1981, Guedes, 2003), so that mass conservation is explicitly enforced. The vortices generated every time step evolve in time in a Lagrangian manner to make up the body wake. The dynamics of the body wake is computed using the vorticity convection-diffusion splitting algorithm, where convection and diffusion are calculated sequentially in time. The convective transport of vorticity is calculated with the Adams-Bashforth second-order time-marching scheme, whereas the diffusive transport of vorticity is simulated using the random walk method. Results for the lift and drag coefficients acting on the cylinder are presented and compared to other results available in the literature for several values of the aspect ratio.

2.Mathematical Formulation

We considere the flow around an ellipti cylinder of length 2*a*, height 2*b* and aspect ratio $\xi \equiv b/a$, immersed in an unbounded region with a uniform flow of freestream speed *U* (Fig. 1). We assume the flow to be incompressible and two-dimensional, and the fluid to be newtonian with constant kinematic viscosity ν. The unsteady flow that develops originates from the boudary layer separation on the cylinder surface, which generates an oscillatory wake downstream of the body. This flow is governed by the continuity and the Navier-Stokes equations in the dimensionless form, which can be written as

$$\nabla \cdot \mathbf{u} = 0 , \tag{1}$$

$$\frac{\partial \mathbf{u}}{\partial t} + \mathbf{u} \cdot \nabla \mathbf{u} = -\nabla p + \frac{1}{Re} \nabla^2 \mathbf{u} . \tag{2}$$

In the equations above $\boldsymbol{u}$ is the velocity vector field, p is the pressure, and $Re \equiv 2Ua/\nu$ is the Reynolds number based on the height of the elliptic cylinder. All quantities in Eqs. (1), (2) and the equations below are nondimensionalized by *U* and *2a*. For all cases studied, the flow is started impulsively from rest. The impermeability and the no-slip boundary conditions on the surface of the cylinder and the condition at infinity can be expressed in terms of the velocity field as

$$u_n \equiv \mathbf{u} \cdot \mathbf{n} = 0 , \text{ on the cylinder surface,} \tag{3}$$

$$u_t \equiv \mathbf{u} \cdot \mathbf{t} = 0 , \text{ on the cylinder surface,} \tag{4}$$

$$|\mathbf{u}| \to 1 , \text{ at infinity,} \tag{5}$$

where $\boldsymbol{n}$ and $\boldsymbol{t}$ are unit vectors normal and tangential to the cylinder surface, respectively. The dynamics of the fluid motion, governed by the boundary-value problem (1)-(5), can be studied in a more convenient way if we take the curl of Eq. (2) and use Eq. (1) to obtain the vorticity equation. For 2-D flows this equation is scalar, and it can be written as

$$\frac{\partial \omega}{\partial t} + \mathbf{u} \cdot \nabla \omega = \frac{1}{Re} \nabla^2 \omega , \tag{6}$$

where ω is the only non-zero component of the vorticity vector, in a direction normal to the plane of the flow.

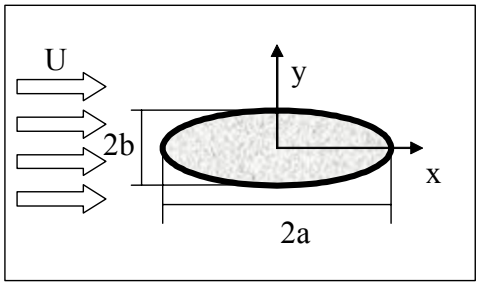

Figure 1: Flow around an elliptic cylinder.

In our model, the flow vorticity is represented by a cloud of N_v discrete point vortices, each of constant strength Γ_j. The contribution to the flow due to the presence of the body is accounted for using a piecewise-continuous linear-source panel method (Anderson, 1991), where the body surface is divided into *N* straight panels, each of strength λ_j. We superimpose the flows comprised of the vortex cloud, the uniform flow and the flow due to the source panels to construct a flow field that satisfies Eqs. (1), (3) and (5) automatically. Thus, the *u* and *v* velocity components of the total flow in the *x* and *y* directions, respectively, can be written in terms of the unknown vortex and source strengths, and the known panel geometry, according to the following equations

$$u(x,y) = \sum_{j=1}^{N} \frac{\lambda_j}{2\pi} \left(\frac{C_u}{2} \ln\left(\frac{Sp_j^2 + 2ASp_j + B}{B} \right) + \frac{D_u - AC_u}{E} \left(\tan^{-1} \frac{Sp_j + A}{E} - \tan^{-1} \frac{A}{E} \right) \right) + \\ -\frac{1}{2\pi} \sum_{j=1}^{N_v} \Gamma_j \frac{(y - y_j)}{(x - x_j)^2 + (y - y_j)^2} \tag{7a}$$

$$v(x,y)=\sum_{j=1}^{N}\frac{\lambda_j}{2\pi}\left(\frac{C_v}{2}\ln\left(\frac{Sp_j^2+2ASp_j+B}{B}\right)+\frac{D_v-AC_v}{E}\left(\tan^{-1}\frac{Sp_j+A}{E}-\tan^{-1}\frac{A}{E}\right)\right)+ \\ +\frac{1}{2\pi}\sum_{j=1}^{N_v}\Gamma_j\frac{(x-x_j)}{(x-x_j)^2+(y-y_j)^2}, \tag{7b}$$

where the constants in Eqs. (7) can be written in terms of the geometrical parameters of the panels, shown in Fig. 2, as

$$A=-(x-Xp_j)\cos\varphi_j-(y-Yp_j)\sin\varphi_j, \tag{8a}$$

$$B=(x-Xp_j)^2+(y-Yp_j)^2, \tag{8b}$$

$$C_u=-\cos(\varphi_j), \tag{8c}$$

$$D_u=x-Xp_j, \tag{8d}$$

$$Sp_j=\sqrt{(Xp_{j+1}-Xp_j)^2+(Yp_{j+1}-Yp_j)^2}, \tag{8e}$$

$$E=\sqrt{B-A^2}=(x-Xp_j)\sin\varphi_j-(y-Yp_j)\cos\varphi_j, \tag{8f}$$

$$C_v=-\sin(\varphi_j), \tag{8g}$$

$$D_v=y-Yp_j. \tag{8h}$$

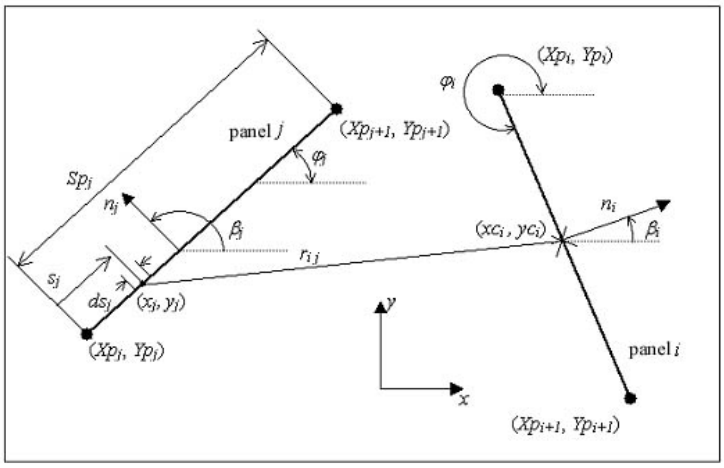

Figure 2: Geometry of the panels.

Equations (7) and (8) are used to calculate the induced velocities at any point in the flow, including the panel control points and the vortices in the wake cloud.

The aerodynamic force coefficients are calculated through the integration of the pressure coefficient distribution on the surface of the elliptic cylinder, which may be expressed as

$$C_D=\int_0^{2\pi\sqrt{\frac{1}{2}(a^2+b^2)}}C_p\sin\varphi(s)ds \quad \text{and} \quad C_L=\int_0^{2\pi\sqrt{\frac{1}{2}(a^2+b^2)}}C_p\cos\varphi(s)ds, \tag{10a,10b}$$

where C_D and C_L are the drag and lift coefficients, respectively., and the pressure coefficient, C_p, on a panel control point (x_{ci},y_{ci}) is calculated according to the following expression

$$C_p=1+2\left(\sum_{n=1}^{m}\frac{\Gamma_n}{\Delta t}-\sum_{n=1}^{n_{\max}}\frac{\Gamma_n}{\Delta t}\right). \tag{11}$$

The index *nmax* refers to the maximum Γ_n value found on the cylinder surface at the stagnation point.

3.Vortex Method Algorithm

The problemformulated above is solved using a Discrete Vortex Method associated with a source panel method. The Discrete Vortex Method uses the convective-diffusive operator-splitting algorithm devised by Chorin (1973), that is

$$\frac{D\omega}{Dt} \equiv \frac{\partial \omega}{\partial t} + \mathbf{u} \cdot \nabla \omega = 0 \tag{12}$$

$$\frac{\partial \omega}{\partial t} = \frac{1}{Re} \nabla^2 \omega \,. \tag{13}$$

In a real flow, vorticity is generated on the body surface so as to satisfy the no-slip condition, Eq. (4), and is transported by convection and diffusion into the flow according to Eq. (6). Our discrete vortex method represents the vorticity by a cloud of discrete vortices, whose Lagrangian transport by convection and diffusion is carried out in a sequence within the same time step. First, the convective process, governed by Eq. (12), is simulated through the calculation of the motion of each vortex. This step is accomplished by integration of each vortex path equation according to the following second-order Adams-Bashforth scheme (Guedes, 2003)

$$\Delta x_c = \left[\frac{3}{2} u(t) - \frac{1}{2} u(t - \Delta t) \right] \Delta t \,, \tag{14}$$

$$\Delta y_c = \left[\frac{3}{2} v(t) - \frac{1}{2} v(t - \Delta t) \right] \Delta t \,. \tag{15}$$

The Adams-Bashforth scheme provides errors of the order of $(\Delta t)^2$, which are smaller than the first-order Euler scheme (errors of the order of Δt). Also, it is faster than the second-order Runge-Kutta scheme because it calculates the velocity field at each vortex position only once per time step, whereas the Runge-Kutta calculates it twice.

In Eqs. (14) and (15), Δx_c and Δy_c are displacements of a vortex owing to convection, and u and v are components of the velocity at the point occupied by the vortex. In order to remove the singularity of the point vortices we use Lamb vortices (Kundu, 1990) for $r \le \sigma$, where σ is the radius of the vortex core at time t. In the first step, the core grows from zero to σ_o, where

$$\sigma_o = 4.48364 \sqrt{\frac{\Delta t}{Re}} \,. \tag{16}$$

The process of viscous diffusion, governed by Eq. (13), is simulated using the Random Walk Method (Lewis, 1991), where the random displacements of each vortex in the x and y directions owing to diffusion, Δx_d and Δy_d, are calculated from

$$\Delta x_d = \Delta r \cos(\Delta \theta) \quad \text{and} \quad \Delta y_d = \Delta r \sin(\Delta \theta) \,, \tag{17a,17b}$$

$$\Delta r = \left[4 Re^{-1} \Delta t \ln(1/P) \right]^{1/2} \,, \text{ and } \quad \Delta \theta = 2\pi Q \,. \tag{18a, 18b}$$

In the Eqs. (18), P and Q are random numbers between 0 and 1 drawn from a uniform probability distribution.

The dimensionless circumferential velocity induced by the j^{th}-Lamb vortex, $u_{\theta j}$ can be written as

$$u_{\theta j} = \frac{\Gamma_j}{2\pi r} \left\{ 1 - \exp\left[-C \left(\frac{r^2}{\sigma_j^2(t)} \right) \right] \right\} . \tag{19}$$

In this particular equation r is the radial distance between the vortex center and the point in the flow field where the induced velocity is calculated, and C = 5.02572 is a constant (Guedes, 2003). The distance ε from the cylinder surface where the nascent vortices are generated per time step (Fig. 3) is set equal to σ_o for all cases studied. Vortices that penetrate the body are reflected back into the flow field. Considering a convective velocity scale of order one and a length scale of order of the average panel length, the time step Δt can be estimated from $\Delta t = (2k/N)(1+\xi)$, where $0 < k \le 2$ is a numerical parameter that limits the convective step of each vortex.

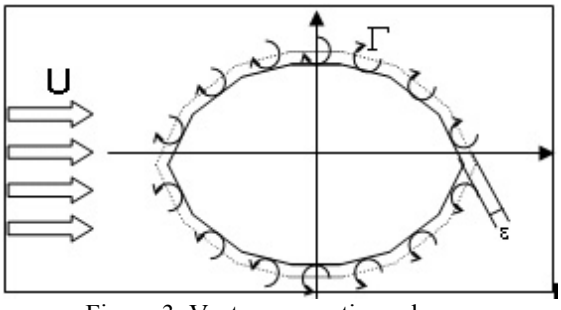

Figure 3: Vortex generation scheme.

4. Numerical Implementation

The body surface is discretized into N small straight panels of different lengths,. The numerical method described above is implemented to run sequentially according to the following steps: (i) generation of N nascent vortices; (ii) calculation of the forces on the body; (iii) convection of the vortices; (iv) diffusion of the vortices; (v) reflection of the vortices that penetrate into the body; (vi) stepping in time.

The process of vorticity generation is carried out so as to satisfy the impermeability and the no-slip conditions, Eqs. (3) and (4). At each time step, N new nascent vortices are created a small distance ε from the body surface, just above of the panel control points (Fig. 3), and N new sources are created along each panel. The strengths of these new vortices and panel sources are determined by imposing the no-slip and the impermeability conditions simultaneously at the N panel control points on the cylinder surface. In order to implement the entire procedure, the velocities induced by all the vortices in the wake are computed at the N control points where Eqs. (3) and (4) must be satisfied. This contribution is added to the right hand side of the algebraic system that includes the normal and the tangential contributions of the incident flow. Hence, $2N$ equations can be written out for the $2N$ unknowns (N new vortex strengths and N new source strengths). We also add two extra equations, which are statements of conservation of circulation (the sum of all vortices with known and unknown strengths must equal zero) and mass (the sum of all new source strengths must equal zero). This procedure yields an algebraic system of $2N$+2 equations and $2N$ unknowns, that is

$$\sum_{k=1}^{N}\left(A_{jk}\Gamma_k(t)+B_{jk}\lambda_k(t)\right)=b_j(t)\,,\quad 1\le j\le N\,, \tag{20}$$

$$\sum_{k=1}^{N}\left(C_{jk}\Gamma_k(t)+D_{jk}\lambda_k(t)\right)=b_j(t)\,,\quad 1\le j\le N\,, \tag{21}$$

$$\sum_{k=1}^{N}\Gamma_k(t)=b_{2N+1}(t)\,, \tag{22}$$

$$\sum_{k=1}^{N}\lambda_k(t)=b_{2N+2}(t)\,, \tag{23}$$

Guedes *et al*. (2004) solves the system above (Eqs. 20 to 23) by relaxing the no-slip and the impermeability conditions written out for the control point at $j = N/2$ (central panel on the cylinder backward face). Hence, removing two equations renders the new $(2N)\times(2N)$ system determined. Although very commonly used in linear systems of algebraic equations obtained from panel methods (Anderson, 1991), this procedure is hard to justify if all equations come from the same source (Strang, 1988). In addition, the usually small error component produced by this scheme adds up as the simulation evolves in time, since one new vortex that does not satisfy both the no-slip and the impermeability conditions is generated every time step. In our new scheme, on the other hand, we remove only the no-slip condition on panel $j = N/2$ to form a $(2N+1)\times(2N)$ system and we use the Singular Value Decomposition Method (Press *et al.*, 1989) to solve it. If the linear system is written in the form $\boldsymbol{Ax} = \boldsymbol{b}$, this method consists of searching for a least squares solution that satisfies the "***normal equations***" (Strang, 1988), *i.e.*,

$$\mathbf{A}^{\mathrm{T}}\mathbf{A}\bar{\mathbf{x}}=\mathbf{A}^{\mathrm{T}}\mathbf{b}\,. \tag{24}$$

Since the columns of the matrix A are linearly independent, the matrix $\boldsymbol{A}^{\mathbf{T}}\boldsymbol{A}$ is an invertible square matrix and $\bar{\mathbf{x}}=(\mathbf{A}^{\mathrm{T}}\mathbf{A})^{-1}\mathbf{A}^{\mathrm{T}}\mathbf{b}$, where the solution vector $\bar{\mathbf{x}}$ is the vector of the unknown Γ's and λ´s that minimizes the error E of the solution in the least squares sense (Strang, 1988), where $E\equiv\left\|\mathbf{A}\bar{\mathbf{x}}-\mathbf{b}\right\|$. The original linear system of algebraic equations $\boldsymbol{Ax} = \boldsymbol{b}$, written in matrix form, is given by

$$\begin{bmatrix} A_{jk} & B_{jk} \\ C_{jk} & D_{jk} \\ 1 & 0 \\ 0 & 1 \end{bmatrix}_{2N+1,2N} \begin{bmatrix} \Gamma_k(t) \\ \lambda_k(t) \end{bmatrix}_{2N} = \begin{bmatrix} b_j(t) \end{bmatrix}_{2N+1}\,. \tag{25}$$

In the $(2N+1)\times(2N)$ matrix A, the $N\times N$ matrix A_{jk} represents the coefficient matrix of the normal velocities induced by all the vortices, the $N\times N$ matrix B_{jk} represents the coefficient matrix of the normal velocities induced by the source panels, the $N\times N$ matrix C_{jk} represents the coefficient matrix of the tangential velocities induced by the vortices, and the $N\times N$ matrix D_{jk} represents the coefficient matrix of the tangential velocities induced by the source panels. Eqations (22) and (23) represent the conservation of vorticity and mass, respectively. The elements of the $(2N+1)\times(2N)$ matrix A depend on the positions of the nascent vortices and of the panel control points on the cylinder surface where the no-slip

and impermeability conditions are imposed, which do not change in time. Therefore, this matrix is calculated only once for the entire simulation. The vector $b_j(t)$ includes the contribution of all the terms in Eqs. (7) and (8) and, therefore, it is recalculated every time step.

5.Results and Analysis

We now present results for four two-dimensional, incompressible, unsteady flow simulations around elliptic cylinders of aspect ratios 0.25 (Case I), 0.5 (Case II), 0.8 (Case III) and 2.0 (Case IV), all for $Re = 1\text{x}10^5$. The numerical parameters used in the computations are: $N = 128$, $\Delta t = 0.1$, $\varepsilon = \sigma_o = 0.0049$ for case I and case IV; $N = 64$, $\Delta t = 0.05$, $\varepsilon = \sigma_o = 0.0032$ for case II and case III; 300 steps (t=30) for case I, 500 steps for the other cases, that results in t = 25 for case II and III and t = 50 for case IV.

(a) Case I: $\xi = 0.25$, $t = 30.0$;

(b) Case II: $\xi = 0.5$, $t = 25.0$;

(c) Case III: $\xi = 0.8$, $t = 25.0$;

(c) Case IV: $\xi = 2.0$, $t = 50.0$;

Figure 4: Positions of the wake vortices of four elliptic cylinders with different aspect ratios for $Re = 1\times10^5$.

The flow around an elliptic cylinder presents several complex phenomena. Experiments show the occurrence of separation, followed by the formation of the so-called Von Karman vortex street, which is comprised of large vortices generated and shed alternately from the upper and lower surfaces of the cylinder. The vortices in the wake are connected in pairs by a vortex sheet, which is represented in the simulation by a sequence of vortices distributed along a line segment. Owing to the periodic characteristics of the wake, the lift force on the cylinder oscillates in time around zero, with a frequency given by the Strouhal number. The periodic behavior of the wake is also reflected on the drag force, which oscillates in time around a non-zero mean value.

The resolution of the method is enhanced by increasing the number of nascent vortices generated at each time step and reducing the dimensionless time step Δt. Increasing the number of generated vortex at each time step means that the vorticity region in the flow will not have holes of potential flow. Reducing Δt means that the solutions of Eqs. (12) and (13) converges to the vorticity equation (Eq. 6).

Figure 4 illustrates the positions of the discrete vortices present in the flow simulation at the final steps of the simulations, for cases I, II, III and IV. These positions are calculated using Eqs. (14), (15), (17) and (18). In all four cases, the wake clearly shows the occurrence of separation at the both sides (up and down) of the elliptic cylinder surface, followed by the generation and growth of large separated vortices near the cylinder, which precedes their shedding into the wake.

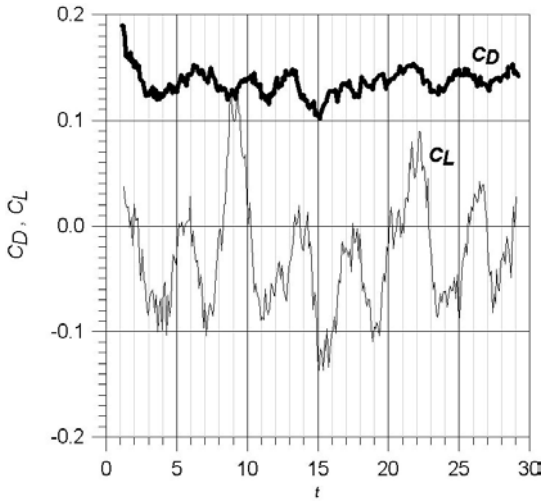

(a) Case I: $\xi = 0.25$

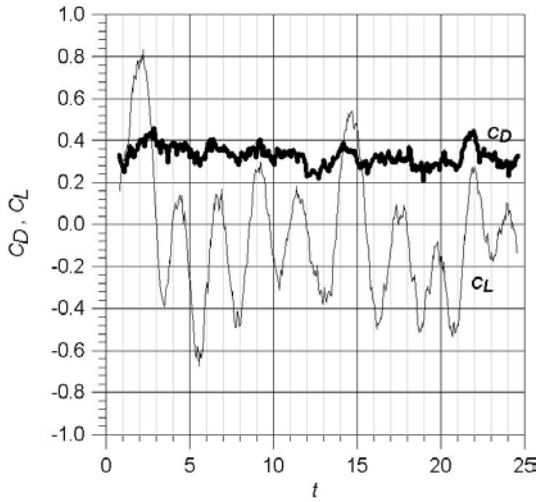

(b) Case II: $\xi = 0.5$

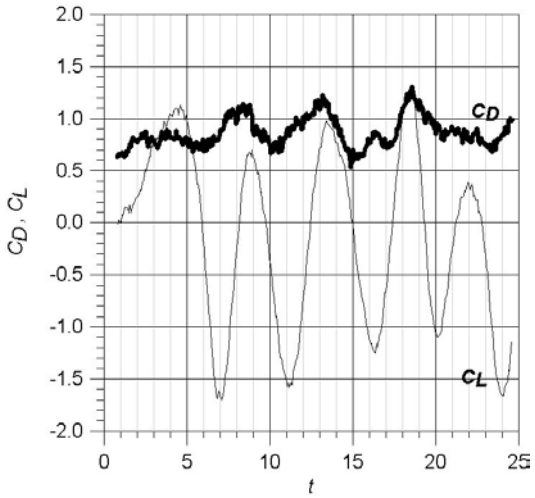

(c) Case III: $\xi = 0.8$

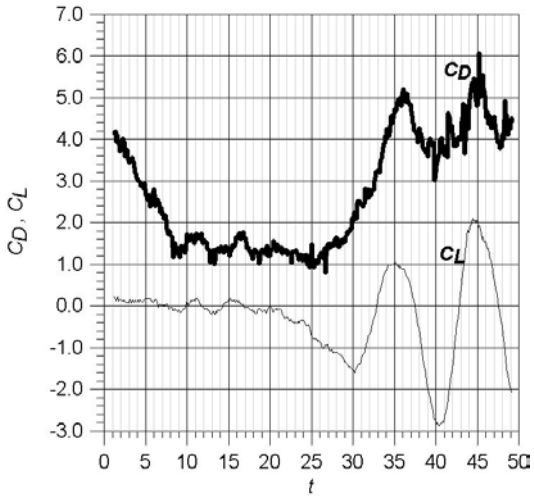

(d) Case IV: $\xi = 2.0$

Figure 5: Time variation of C_D and C_L for $Re = 1\times10^5$.

The time histories of the lift and drag coefficients are revealed in the graphs of Fig. 5, for all four cases studied. The lift coefficient oscillates about zero with a non-dimensional frequency, or Strouhal number, given by: $St = 0.06$, for case I, calculated over 5 cycles of oscillation corresponding to the C_L peaks between $t = 7.0$ and $t = 28.0$; $St = 0.20$, for case II, calculated over 7 cycles between $t = 5.5$ and $t = 23.0$; $St = 0.19$, for case III, calculated over 4 cycles between $t = 7.0$ and $t = 24.0$; and $St = 0.20$, for case IV, calculated over 1 cycle between $t = 35.0$ and $t = 45.0$. On the other hand, the drag force oscillates about a mean value calculated to be $C_D = 0.13$, for case I, $C_D = 0.32$, for case II, $C_D = 0.90$, for case III and $C_D = 4{,}30$, for case IV, all integrated over the same cycles used to determine St.

Table 1 provides an easy way to compare our numerical results for the drag coefficient and Strouhal number to other experimental and numerical results available in the literature. For case I, the mean drag coefficient is 43% lower than the experimental one obtained from Blevins (1984), and the Strouhal number is 30% lower. For case II the mean drag coefficient is 53% lower than the experimental one, and the Strouhal number is the same. On the other hand, cases III and IV, our results show a difference of about 33% and 63% respectively for the mean drag coefficient and approximately the same values of the experimental one for the Strouhal number. The best results are those for case III and IV, because there is no discrepancy for the Strouhal number, and the calculated value of the mean drag coefficient is higher than the experimental value. Regardless of the overall good comparison observed, our numerical results indicate that the algorithm still needs investigation in order to yield more accurate results.

Table 1. Comparison of the drag coefficient and Strouhal number with other numerical and experimental results.

Results	Aspect Ratio	*Re*	C_D	*St*
Blevins (1984): experimental	0.25	$1x10^5$	0.30	≈ 0.20
Carreiro & Bodstein (2002): numerical	0.25	$1x10^4$	0.21	0.93
Present results: numerical	0.25	$1x10^5$	0.13	0.06
Blevins (1984): experimental	0.5	$1x10^5$	0.60	≈ 0.20
Carreiro & Bodstein (2002): numerical	0.5	$1x10^4$	0.49	0.46
Present results: numerical	0.5	$1x10^5$	0.32	0.20
Blevins (1984): experimental	0.8	$1x10^5$	0.64	≈ 0.20
Carreiro & Bodstein (2002): numerical	0.8	$1x10^4$	0.89	0.21
Present results: numerical	0.8	$1x10^5$	0.90	0.19
Blevins (1984): experimental	2.0	$1x10^5$	1,60	≈ 0.20
Present results: numerical	2.0	$1x10^5$	4.30	0.20

6.Conclusions

A mesh-free two-dimensional discrete vortex method coupled with a source panel method is implemented to calculate the Strouhal number and the lift and drag coefficients on four elliptic cylinders, each with a different aspect ratio, in a two-dimensional, incompressible, unsteady and high Reynolds number flow.

As the simulations show, the numerical results obtained are in overall good agreement with the experimental results used for comparison, especially for the Strouhal number in the simulations for the cylinder with aspect ratio equal to 0.5 or higher. The discrepancies observed in the determination of the Strouhal number and the drag coefficient for the elliptic cylinder with aspect ratio of 0.25 may be attributed to difficulty in simulating the dynamics of the vortex shedding with enough resolution of the vorticity field. Although the algorithm has proven to be very effective to simulate massively separated flows around elliptic cylinders, the numerical results suggest that the panel distribution scheme must be more thoroughly explored. An increase in the resolution of the simulation, through an increase of the number of vortices, may also attenuate the problems encountered in the cases studied. The numerical parameters used also require further tests to find more adequate values. However, it must be pointed out that the numerical calculation of massively separated flow is expected to be difficult due to the flow complexity. This fact is corroborated by the relatively large discrepancies between experimental results available in the literature, when compared to each other. The use of a fast summation scheme to determine the vortex-induced velocities, such as the Multipole Expansion scheme, allows an increase in the number of vortices and a reduction of the time step, which increases the resolution of the simulation, reduces the CPU time and provides the means for longer-time simulations to be carried out.

7. References

1. Anderson, J.D., 1991. "Fundamentals of Aerodynamics", 2nd. Edition, McGraw Hill.
2. Blevins, R.D., 1984, " Applied Fluid Dynamics Handbook", Van Nostrand Reinhold Co.
3. Carreiro, F dos R. and Bodstein, G.C.R., 2002, "Simulação Numérica do Escoamento Não-Permanente em Torno de Cilindros Elípticos Via Transformação de Joukowsky", 9th Brazilian Congress of Thermal Engineering and Sciences - Encit 2002, Caxambu, M.G., pp. 1-10.
4. Chorin, A.J., 1973, "Numerical Study of Slightly Viscous Flow", Journal of Fluid Mechanics, Vol. 57, pp. 785-796.
5. Fusen HE and Tsung-Chow Su, 1998, "A Numerical study of bluff body aerodynamics in high Reynolds number flows by viscous Vortex Element Method", Journal of Wind Engineering and Industrial Aerodynamics, Vols.77 e 78, pp.: 393-407.
6. Guedes, V.G., Bodstein, G.C.R. and Hirata, M.H., 2004, "Numerical Simulation of the flow around a square cylinder using the vortex method",Revista de Engenharia Térmica, RETERM, v.3, nº 2, pp. 161-167.
7. Guedes, V.G., 2003, "Numerical Simulations of flow around circular and rectangular cylinders using the vortex method", D.Sc. Thesis PEM - COPPE / UFRJ.
8. Leonard, A., 1980, "Vortex Methods for Flow Simulation", Journal of Computational Physics, Vol. 37, pp. 289-335.
9. Kundu, P.K., 1990, "Fluid Mechanics", Academic Press.
10. Lewis, R.I., 1991, "Vortex Element Methods for Fluid Dynamic Analysis of Engineering Systems", Cambridge University Press, Cambridge.
11. Pereira, L.A.A., Ricci, J.E.R., Hirata, M.H.H. and Silveira Neto, A., 2002, "Simulation of vortex-shedding flow aound a circular cylinder with turbulence modelling", Computational Fluid Dynamics Journal, v. 11, nº 3, pp. 315-322.
12. Press, W.H., Flannery, B.P., Teukolsky, S.A. and Vetterling, W.T., 1989, "Numerical Recipes - the Art of Scientific Computing (Fortran Version)", Cambridge University Press.
13. Strang, G., 1988, "Linear Algebra and Its Applications", Harcourt Brace.